Mechanisms of Electron Transfer Rate Modulations in Cytochrome P450 BM3.

Vaibhav A. Dixit,^{§*} Upadhyayula Suryanarayana Murty,[§] Priyanka Bajaj,[⊥] Jochen Blumberger,[&] and Sam P. de Visser[‡]

- § Department of Medicinal Chemistry, National Institute of Pharmaceutical Education and Research, Guwahati, (NIPER Guwahati), Department of Pharmaceuticals, Ministry of Chemicals & Fertilizers, Govt. of India, Sila Katamur (Halugurisuk), P.O.: Changsari, Dist: Kamrup, Pin: 781101, Guwahati, Assam, India
- ¹ National Institute of Pharmaceutical Education and Research, Hyderabad (NIPER Hyderabad), NH-9, Balanagar Main Road, Kukatpally Industrial Estate, Balanagar, Hyderabad, Telangana. 500037, India
- & Department of Physics and Astronomy, and Thomas Young Centre, University College London, Gower Street, London WC1E 6BT, United Kingdom
- [‡] Manchester Institute of Biotechnology and Department of Chemical Engineering, The University of Manchester, 131 Princess Street, Manchester M17DN, United Kingdom

KEYWORDS: Electron Transfer, Marcus Theory, CYP450 BM3, Molecular Dynamics.

ABSTRACT: The bacterial cytochromes P450 BM3 (CYP450 BM3) catalyzes reactions of industrial importance. Despite many successful biotransformations, robust re(design) for novel applications remains challenging. Rational design and evolutionary approaches are not always successful highlighting a lack of complete understanding of the mechanisms of electron transfer (ET) modulations. Thus, the full potential of CYP450 reactions remains under-exploited. In this work, we report the first MD-based explicit prediction of BM3 ET parameters (reorganization energies; λ and ET free energies; Δ G°), and log ET rates (log $k_{\rm ET}$) using Marcus theory. Overall, the calculated ET rates for the BM3 wild-type (WT), mutants (F393 and L86), ligand-bound state, and ion concentrations agree well with experimental data. In ligand-free (LF) BM3, mutations modulate $k_{\rm ET}$ via ET Δ G°. Simulations show that the experimental ET rate enhancement is due to increased driving force (more negative Δ G°) upon ligation. This increase is related to the protein reorganization required to accommodate the ligand in the binding pocket, rather than binding interaction with the ligand. Our methodology (CYPWare 1.0) automates all the stages of MD simulation step-up, energy calculations, and estimation of ET parameters. CYPWare 1.0 and this work, thus represent an important advancement in the CYP450 ET rate predictions which has the potential to guide the redesign of ET enzymes. This program and a web tool are available on GitHub for academic research.

INTRODUCTION

The cytochromes P450 (CYP450) are important enzymes in biosystems and are found in almost all forms of life.1-10 They are involved in biodegradation pathways of, for instance, xenobiotics in the human liver, but also take part in essential biosynthesis reactions of natural products, such as hormones.¹¹⁻¹³ In biotechnology, not surprisingly, the CYP450s have emerged as important greener alternatives for performing many biochemical transformations of industrial importance. Examples include the biosynthesis of hydrocarbons from fatty acids to generate biofuels.14-17 In addition, a cytochrome P450 from Bacillus megaterium (namely CYP450 BM3) has been developed as a tool for performing selected reactions giving access to chiral chemicals, drug metabolites, and intermediates. 1,7,18 Large libraries of CYP450 mutants have been developed and designed for performing unusual aliphatic and aromatic hydroxylation reactions, as well as carbene insertion reactions. Although site-directed mutagenesis and directed evolution have been

successful in many chemical and drug intermediate syntheses, demand-based timely delivery of mutants with desired activities and selectivities remains challenging and only partially successful. Moreover, only retrospective analysis of experimental stereo and regioselectivity and substrate specificities are put forward using crystal structure analysis which mostly focuses on the active site interactions and complementarity.⁴ Such retrospective analysis mostly attempts to explain observed selectivity based on close contacts (favourable or unfavourable) between the ligands (substrates) and the CYP450 active sites.

Kanoh et al., have recently developed an experimental mutant screening criterion based on existing methodologies that focus on 1) typical ligand binding, followed by 2) Type I spectral change, 3) rapid coupled oxidation (nature of coupling is not mentioned explicitly), and 4) conversion to a limited number of products.⁵ At each step false positives from the previous steps are identified and filtered out.

Although this methodology and selection criteria did identify a few exemplary substrates, it requires multiple incubations with different CYP450 enzyme systems and strong analytical method development, validation expertise, and support, thus making it resource and fund-intensive. Applications of this screening methodology in a real-time search for CYP450 mutants with novel reactivity need to be further demonstrated and tested.

Although the natural substrates (ligands) for CYP450 BM3 are long-chain (C₁₂-C₂₀) saturated fatty acids, evolved mutants can accept low molecular weight fatty acids, alkanes, ethyl diazocarboxylate for cyclopropanation, amination of C-H bonds in addition to stereoselective C-H hydroxylations (Figure 1).6,7 Natural substrates undergo stereoselective terminal ω -1, 2 or 3 hydroxylations with the wild type BM3.8 Unsaturated fatty acids are hydroxylated with higher (almost exclusive) regioselectivity compared to saturated analogues (Table 1 of reference 8). The reduced conformational freedom associated with the fixed configurations around double bonds might partially explain these observations. MD simulations and QM/MM calculations and analysis of the potential energy diagram for Compound I (Cpd I) catalyzed reactions have been used by Shaik et al., to explain the regio and stereoselectivity in BM3 hydroxylations starting from the crystal structure (1JPZ).9 Such retrospective analysis is not feasible for most of the mutants and protein-ligand pairs for which a crystal structure is not yet available. Moreover, as recognized in the BM3 literature, a larger active site and flexibility of this enzyme (expectedly) makes it difficult to objectively rationalize subtle changes in substrate selectivities observed with changes in and around the active site. 10 Molecular docking can be used to find potential substrates, and potential sites of metabolism (SOM) in substrates, and get insights into the mechanisms of CYP450 inhibition. 11-13 Nonetheless, limitations of docking methodologies in consistently ranking potential ligands from structurally diverse datasets for a larger subset of protein targets are well recognized in the literature.¹⁹ Thus docking protocols usually require extensive validation for conformational sampling and scoring functions which often require tailoring for specific protein classes. Docking often produces 2-3 degenerate poses (≤ 1 kcal/mol) with very different molecular orientations within the active sites. Thus, in a computational analysis, choosing only one protein or ligand crystal structure or a docked pose where experimental SOM is within a cut-off distance from Heme-Fe (typically < 6.0 Å), can be considered an oversimplified, biased, or incomplete treatment of the problem. An unbiased analysis ideally requires ensemble docking²⁰ or should include at least the top 2-3 poses. Alternatively, all the top poses within two standard deviations of the scores among all the legitimate poses produced (i.e., representing the Boltzmann distribution) can be considered. Although this might be computationally expensive forcing trade-offs between accuracy and speed.

Modulations of CYP450 activities do not necessarily require mutations within the active site⁷ and in many cases, mutations in the protein sequence are not essential. For

example, buffer ion concentrations used in in-vitro systems have been demonstrated to influence electron transfer (ET) rates in CYP450 BM3. Gilardi et al., have observed bellshaped relationship between the ionic strength of the buffer solution and CYP450 BM3 reduction rates.¹⁴ Similarly Gemzik et al., have reported the modulation of rat CYP450 activities by buffer ionic strengths and pH.15 Earlier we performed an analysis of CYP450cam crystal structures for the presence of buffer ions in close proximity to the catalytic center.¹⁶ Fifty-two structures contain a potassium ion that interacts via the ligand and protein backbone atoms with the Heme center (Fe to K+ distance < 14 Å). Thus, the influence of these close buffer ions interactions with truncated Heme models was studied to estimate the ET free energy (ΔG°) , often called the driving force, using DFT calculations. 16 Single monovalent alkali metal ions within 14 Å of the Heme consistently stabilized the reduced (Ferrous) state thus increasing the ΔG° for the ET, whereas two such ions caused overstabilization and brought the Heme complex into the inverted-Marcus regime thus reducing the ET rates. Divalent alkaline earth metal ions also over-stabilized the reduced state and entered the inverted-Marcus regime and reduced the ET rates. This suggests that the total charge within an interacting distance of the catalytic center can have a strong influence on reactivity. In that work, protein, and solvent reorganization energies (λ_{prot} , and λ_{solv}) were considered constant (0.76 eV) while studying the influence of the alkali metal ions. Although this is a reasonable approximation for studying the influence of small ligands or buffer ions, mutations and varying active site interactions often alter the λ_{prot} and λ_{solv} values in a different way and consequently can influence the ET rates.²¹⁻²⁴ Thus explicit calculation of these ET terms is essential for a reasonably accurate estimation of ET rates in BM3 in different environments, with mutations and different ligands. Such a reliable estimation of CYP450 ET rates, activities, and selectivities can significantly minimize the time required for the evolution of CYP450 mutants with desired properties.

Recently MD simulations of the resting state have been used for retrospective analysis of the influence of ligand binding on co-factor distance and interactions with the redox partner. Shaik et al. have performed MD simulations on the crystal structure of BM3 (1BVY) in which the Heme domain of BM3 called BMP is expected to be fused with the redox partner (FMN containing reductase often called BMR).²⁵ The cofactors (FMN and Heme) moved even closer (minimum distance of 12 and 8.8 Å) during the MD and QM/MM optimization. Earlier Verma et al., have performed MD simulations and employed Pathways program in VMD²⁶ to estimate the ET rates ($k_{\rm ET}$) in WT BM3 using the same protein structure (1BVY).27 These authors also did not build the missing linker (see reference 27) and used approximate values for the ET ΔG° and λ for $k_{\rm ET}$ calculations. Although the potential ET pathways were analysed for every 10 ns, no attempts were made to explicitly calculate ET parameters, and objectively and/or retrospectively identify pathways that allow ET rate predictions in mutants or upon ligand binding.

In recent years, empirical or semi-empirical Marcus theory coupled with molecular dynamics (MD) simulations has been utilized for a reasonably accurate estimation of ET rates in multi-Heme bacterial cytochromes²⁸⁻³¹ and Hemoglobins.³² Details of the underlying theory and approach are given in the Methods section. Nonetheless, explicit estimation of λ_{prot} , and λ_{solv} , reorganization energies in CYP450s using MD simulations have not been undertaken thus far and thus insights into these crucial ET parameters for a biotechnologically important protein remain missing in the literature. Similarly, extensive investigations and analysis of Marcus electron transfer (ET) free energies and rates for the CYP450 isoforms (bacterial or human) are also missing. Only two papers discussed above utilized Dutton's empirical²⁵ and Pathway²⁷ model for approximate estimation of ET rate in WT BM3.

In this manuscript, we report the first MD-based calculations of ET reorganization energies (λ_{prot} , and λ_{solv}), free energies, and ET log rates for the CYP450 BM3 catalyzed reactions. We address the following questions to get insights into the biochemistry of CYP450 BM3 reactions, 1) What are ET parameters; reorganization energies λ_{prot} , and λ_{solv} , and free energies (ΔG°) for the ligand-free (LF) BM3? 2) How does ligand binding influence ET parameters. 3) Can MD simulation-based estimation of ET parameters and semiclassical Marcus theory predict experimental ET rates for CYP450 BM3 WT and ligand-bound complexes? 4) Can MD simulations model the dependence of ET λ_{solv} and rates on ionic strength? 5) How do mutations in the CYP450 BM3 influence the ET parameters and rates?

METHODS

Computational details

The ET reaction between two cofactors can be modelled with a simple reaction shown in *Equation 1*.

$$RO(a) \rightarrow OR(b)$$

Equation 1

Where R and O represent the reduced (electron donor) and oxidized (electron acceptor) states of the cofactors in the redox proteins. For CYP450 BM3, the R and O are fused by the linker and represent reductase (FMN: BMR) and CYP450 (Heme: BMP) domains involved in ET and ligand recognition. The RO and OR states are often referred to simply as states a and b respectively. The energies of diabatic electronic states are $E_a(\mathbf{R}^N)$ and $E_b(\mathbf{R}^N)$, where \mathbf{R}^N is the 3D configurational vector for a system with N atoms. These energies are two of the elements of the electronic Hamiltonian matrix of this system, whereas H_{ab} represents electronic coupling between the cofactors (equation 2 in reference ³³). The difference between $E_a(\mathbf{R}^N)$ and $E_b(\mathbf{R}^N)$, is the vertical energy gap which is used as a reaction coordinate to simulate ET free energy curves (see reference 33). In the semi-classical Marcus ET theory, which combines concepts from the transition state theory of chemical reactions and Landau-Zener electronic transition theory,34 the free energy of the system is defined by the difference in energy of the two diabatic states i.e., energy gap (ΔE). When ΔE is negative, ET is favored from the RO(a) to the OR(b) state. The thermal fluctuations in these states allow the electron to tunnel (jump) between the cofactors. The thermal average of vertical energy gaps for the two states (ΔE_a and ΔE_b) gives the free energy difference (ΔG°) or the driving force for the ET, whereas the half of difference in vertical energy gaps is the reorganization energy (see Equation 2). The point at which the two diabatic free energy curves (RO and OR) meet represents the classical barrier for the ET (Equation 2). Application of the semi-classical Marcus theory then allows the prediction of ET rates using Equation 3.

$$\lambda = \frac{(\Delta E_a - \Delta E_b)}{2}$$
, $\Delta G^{\circ} = \frac{(\Delta E_a + \Delta E_b)}{2}$, $\Delta G^{\ddagger} = \frac{(\lambda + \Delta G^{\circ})^2}{4*\lambda}$,

Where, $\Delta E = E_b - E_a$

Equation 2

$$k_{ET} = \frac{2\pi}{\hbar} * |H_{ab}|^2 * (4\pi\lambda k_B T)^{-1/2} * e^{\left(\frac{-(\lambda + \Delta G^{\circ})^2}{4\lambda k_B T}\right)}$$

Equation 3

where H_{ab} is the electronic coupling matrix between the cofactor estimated from distance dependence reported earlier, 28,32 k_B is the Boltzmann constant, T temperature in Kelvin and \hbar is the reduced Planck's constant.

Protein preparation

CYP450 BM3 crystal structure (1BVY) was downloaded from PDB website.35 As mentioned above, this structure lacks the coordinates for the linker connecting the Heme (BMP) and Flavin (BMR) domains of the BM3. Our attempts to model the linker with Modeller 10.2 did not give good quality structures (see Figure S1),36,37 Thus the linker was modelled as a linear peptide sequence (generated with tleap) and was inserted manually between BMP and BMR chains of 1BVY structure (see supporting information). The protein chain protonation states were determined by the H++ 3.0 webserver (pH = 7.4). Heme cofactor was parameterized using the MCBP.py tool⁴⁰ where charges and force constants were calculated using Gaussian09 at B3LYP/6-31G(d) level.41 The procedure for parameterization is like that reported earlier for the Hemoglobin³² and the penta mutant CYP450 example reported on Amber tutorial website.⁴² The reduced and oxidized forms of both the cofactors were modelled by choosing the correct spin state and charges (Heme Ferric/oxidized state: charge = -2 and doublet multiplicity whereas for the Ferrous/reduced state: charge = -3 and quintet multiplicity.8 The FMN cofactor was modelled as a semiquinone undergoing one-electron oxidation and was parameterized with antechamber program of AmberTools20. The protein structure thus prepared was subsequently minimized and equilibrated for MD studies using AmberTool20 and Amber20.43 Ligands were also parameterized with antechamber program.

Molecular docking with AutoDock Vina

The typical BM3 substrates, Arachidonic (ACD), Lauric (LAU), Palmitic (PAL), and Myristic (MYR) acids, were docked into the active site of the Heme domain (BMP). For this, the ligand structures were prepared as follows. Two dimensional SDF files were downloaded from PubChem CID (Arachidonic acid: 444899, Lauric acid: 3893, Palmitic acid: 985 and Myristic acid, 11005). Openbabel was used to convert these into 3D mol2 files with Gasteiger charges and finally converted into PDBQT format.⁴⁴ The protein structure prepared in AmberTools20 was saved in the PQR format and converted into PDBQT format using an in-house shell script. Molecular docking was performed using AutoDock Vina.⁴⁵ The grid center was defined as a point 6 Å above the Heme plane, with a grid size of 25 * 25 *25 and exhaustiveness = 8.

Molecular dynamics (MD) simulations

Explicit MD simulations on both redox states were run in triplicate (starting from the equilibrated protein structure) for each ligand-free (LF) and ligand-bound (LB) BM3 followed by estimation of vertical energy gaps (ΔE).^{32,33} Top 3 docked poses were considered for running 20 ns MD simulations and ET parameter calculations. Thus, a total of 360 ns long simulations were run for each substrate-bound complex. An in-house program (CYPWare 1.0) was developed to integrate and automate various steps required to perform GPU-enabled MD simulations in Amber 20. These include 1) parameterization of the ligand with antechamber, 2) preparation of ligand-BM3 complexes for a userspecified pose, 3) generation of input files for tleap, pmemd, sander calculations, 4) creation of parameter, topology files for MD simulations, 5) minimization, heating, and equilibration with AmberMDPrep,466) running GPU enabled MD simulations, trajectory analysis, extracting Amber force fieldbased single-point energies, and co-factor distances and 7) calculation of vertical energy gaps (ΔE), ET free energy (ΔG°) , protein and solvent reorganization energies $(\lambda_{\text{prot.}})$ and λ_{solv}). The procedure used in step 7 remains similar to that reported earlier for the Hemoglobin³² variants and it has been automated during the development and implementation of CYPWare 1.0. Briefly, the average Amber FF energies during the MD production runs were calculated using the parameters for both the redox states (E_a and E_b) for

MD trajectories of the two redox states. The difference in these energies is the vertical energy gap, $\Delta E = E_a - E_b$. The reorganization energies (λ) and the ET ΔG° are calculated using Equation 2. The ET ΔG° for the wild-type (WT) BM3 was shifted to the experimental driving force for the LF state (0.039 eV, see the next section). The ET ΔG° for the BM3 complexes (LB WT BM3, mutant BM3, LB mutant BM3, and different ion concentrations) were estimated by adding the WT ET ΔG° to the difference in Amber FF based ΔG° for the wild-type BM3 and complexes (see Equation 4). The λ values were scaled by a factor of 1/1.6 to account for the missing electronic polarizability in the force field used.³³ These parameters were then fed into the semi-classical Marcus equation (Equation 3) to calculate the ET rates ($k_{\rm ET}$) and log ET rates with respect to the WT BM3.

$$\Delta G^{\circ}(BM3\ comp) = 0.039 + (\Delta G_{FF-BM3\ comp}^{\circ} - \Delta G_{FF-WT\ LF}^{\circ})$$

Equation 4

Where $\Delta G^{\circ}_{FF\text{-}WT\ LF}$ is the Amber force field (FF) based ET free energy (Equation 2) for the WT ligand-free (LF) state, $\Delta G^{\circ}_{FF\text{-}BM3\ complex}$ is the FF based ET free energy for the BM3 complexes.

RESULTS AND DISCUSSION

Validation of docking protocol: Pose and Affinity prediction.

Validation of a docking protocol usually includes reproducing crystal structure pose and correctly ranking a series of ligands with respect to binding affinities. Among the most typical BM3 substrates, only two crystal structures for natural BM3 substrate (i.e., Palmitic acid) are known in the PDB database (4ZFB and 2UWH). The structure 2UWH contains mutation (A82F) where Phe82 is in the proximity of the hydrophobic tail of the bound ligand. The 4ZFB structure is an unstable pentamutant. Both structures retain an H-bonding interaction between the carboxylate and phenolic hydroxyl of the Y51 residue. Since the 4ZFB represents an unstable mutant, 2UWH was chosen for assessing the ability of the docking protocol to find native binding mode.

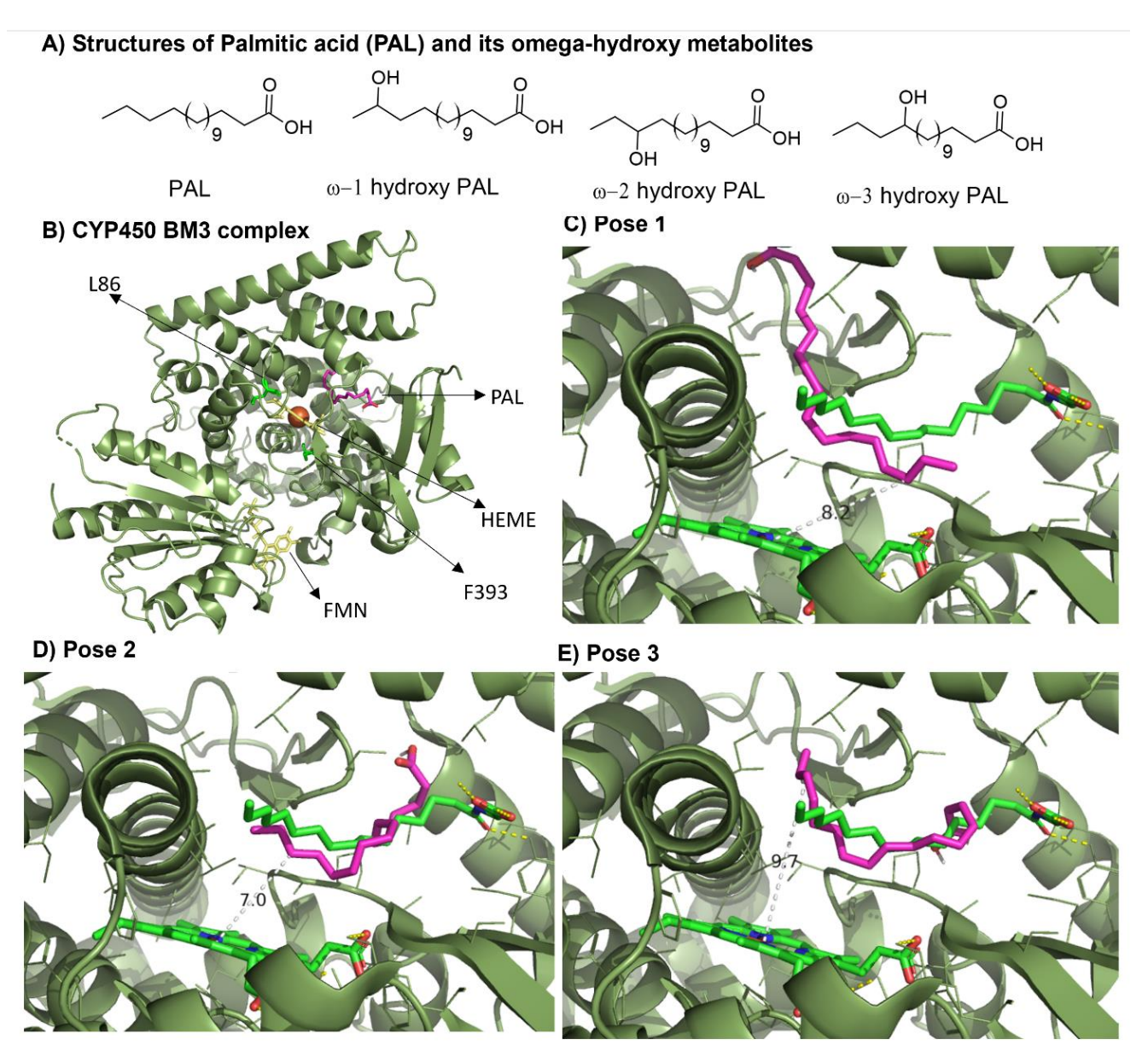


Figure 1. Structures of CYP450 BM3 substrate palmitic acid (PAL), its metabolites, and CYP450 BM3 complex, and docked poses of PAL in the active site. A) The structure of PAL and its omega-1,2 and 3-hydroxy metabolites. B) Heme and FMN are shown in yellow colour, while the sites of mutations studied in this work are shown in green. Also, top 3 docked poses (magenta) compared with the crystal structure pose (green) for Palmitic acid (2UWH) are shown in C, D, and E panels. C) The First pose shows an alternative placement of the fatty acid which brings SOM within similar contacts with Heme. D) The Second pose shows the placement of the carboxylate and side-chain comparable to the crystal structure pose. E) Third pose also brings SOM atoms like the positions seen in 2UWH. Thus, these Top 3 poses were considered for MD simulations, ET parameter and rate predictions.

Table 1. Vina docking scores of the top three poses and dissociation constants (K_d, experimental and predicted), for typical BM3 substrates.

Ligand	Pose Number	Vina Score (kcal/mol)	K _d (uM) ^a	K _d (predicted) ^b
	1	-6.9		
Arachidonic acid (ACD)	2	-6.7	3	13
	3	-6.5		
	1	-5.2		
Lauric acid (LAU)	2	-5.1	240	203
	3	-4.9		
	1	-5.8		
Palmitic acid (PAL)	2	-5.8	10	63
	3	-5.7		
	1	-5.4		
Myristic acid (MYR)	2	-5.1	78	137
	3	-5.1		
	1	-6.2		
N-palmitoyl glycine (NPG)	2	-6.1	0.082^{c}	38
	3	-5.9		

^a K_d values are from Table 2 of reference ⁸

Figure 1 shows the top three docked poses for Palmitic acid (PAL) generated by AutoDock Vina. All the top 3 poses show the reported SOMs (omega-1, 2 and 3 carbons) in positions similar to crystal structure poses and also within 10 Å of the Heme Fe.⁸ Considering a large number of rotatable bonds (n = 14) in PAL and active site volume for BM3, these can be considered a good agreement with the experimental data (Table 1). These SOMs move about 2 Å away from the Heme ring during the MD simulations (see Figures S3 and S4). This drift in ligand position is considered essential for the subsequent step in the catalytic cycle namely dioxygen binding. For Arachidonic acid (ACD) the SOM-Fe distances are larger than 10 Å in the top 3 poses and remain so during the MD simulations of redox states. The Vina score-based calculations of the dissociation constant (K_d) for these substrates are within an order of magnitude of the experimental data reported in the literature (except for NPG, see Table 1 above, Figure S5, and Table 2 in reference 8). NPG is a relatively polar ligand and entropic, and desolvation effects are expected to drive the binding thus standard docking protocol is unable to correctly predict binding affinity but nonetheless places the ligand in an orientation very similar to the crystal structure pose (1JPZ, see Figure S2). These findings validate our docking protocol in terms of both pose and approximate affinity predictions for typical BM3 ligands. Thus, the top 3 docked poses were selected for further MD simulations and ET parameter analysis. The influence of using the crystal structure coordinates vs docking pose on calculated ET parameters is discussed later in the manuscript.

ET parameters for the ligand-free (LF) BM3 and F393, L86E mutants

Experimental redox potentials for the BM3 wild-type, FMN domain of the reductase, and selected BM3 mutants are known in the literature.^{8,50,51} These give a reasonable estimate for the electron transfer free energy (ΔG°) i.e., the driving force in the semi-classical Marcus equation (*Equation 3*). For the ligand-free (LF) WT BMP (Heme) and the

BMR (FMN) domains the experimental redox potentials (E°) are -0.427 V and -0.388 V. 50,51 The ET ΔG° for the reduction of BM3 Heme by FMN calculated from these values is 0.039 eV. These should be considered an approximation since such E° are mostly measured for the isolated Heme and FMN domains and interactions with redox partners can modulate these values.

As mentioned in the introduction, Shaik et al. used crystal structure (1BVY) to empirically model ET rates using cofactor distance from MD simulations.²⁵ The CYP450 BM3 (BMP) is expected to be fused with the redox partner containing the FMN cofactor (BMR). But as mentioned by the authors of the original crystal structure (1BVY) the linker peptide fusing the BMP and BMR domains gets proteolyzed during protein purification. Thus the crystal structure 1BVY (http://doi.org/10.2210/pdb1BVY/pdb) lacks this linker.⁵² The methodology section and supporting information of Shaik's paper do not mention building/modeling the missing linker, rather they have overlayed the BMP domain of 1JPZ with that of the 1BVY to insert the ligand (Npalmitoylglycine: NPG) into the Heme active site of 1BVY structure. The Heme and FMN cofactors moved closer (min 12, max 20 Å) during the MD simulation in the ligand-bound (LB) Ferric high spin state compared to the ligand-free (LF) state (min 12, max 24 Å, see Figure 1 in reference ²⁵). The cofactors moved even closer (8.8 Å) during the QM/MM optimization of the most populated structure. This closest approach may be an artifact of the missing linker as this seems to have allowed an artificially closer approach between the two domains not observed experimentally. Additionally, the protein and solvent reorganization were not estimated explicitly but a constant value for the total ET λ = 0.76 eV was assigned.

 $^{^{}b}$ K_d values predicted from average Vina score for top 3 poses and ignores the entropy and desolvation factors, where ΔG° = RT ln (K_d).

 $^{^{\}text{c}}$ Kd value taken from reference 49

Table 2. Average cofactor minimum distance (Heme to FMN), electron transfer (ET) reorganization energies (λ , eV), protein and solvent contributions to λ (λ_{prot} and λ_{solv}), free energy (ΔG° , eV) for the reduction

of BM3 Heme by FMN, calculated and experimental relative logarithmic ET rates for the LF BM3 variants (wild type, F393A and F393W mutants).

Sr. No.	BM3 mutant	Avg cofactor min distance (Å)	ΕΤ λ	$\lambda_{ m prot}$	$\lambda_{ m solv}$	ET ∆G°*	Cal. log k _{et}	Exp. log k _{et}
1	WT	14.57 ± 1.33	1.15 ± 0.05	0.56 ± 0.10	0.59 ± 0.15	0.039	1.24	0.70
2	F393A	14.46 ± 1.33	1.18 ± 0.02	0.42 ± 0.12	0.76 ± 0.15	0.094 ± 0.01	0.57	0.49
3	F393W	14.34 ± 1.19	1.15 ± 0.02	0.56 ± 0.10	0.59 ± 0.12	0.082 ± 0.01	1.28	1.04
4	L86E	14.32 ± 1.31	1.12 ± 0.02	0.58 ± 0.09	0.54 ± 0.12	0.000 ± 0.01	1.96	2.01

^{*} ET ΔG° for mutants are scaled to the experimental data for WT BM3.

Table 3. Average cofactor minimum distance (Heme to FMN), electron transfer (ET) reorganization energies (λ , eV), protein and solvent contributions to λ , free energy (ΔG° , eV), calculated and experimental

relative logarithmic ET rates for the BM3 variants (WT, F393A and F393W mutants). Values are the average of 3 MD runs for the top 3 docked poses.

Sr. No.	BM3 WT/Mutant ligand pair	Cofactor dis. (Å)	λ_{prot}	$\lambda_{ m solv}$	ΕΤ λ	ET ΔG°*	Cal. log k_{ET}	Exp. $\log k_{ET}$
1	WT-ACD	14.58 ± 1.14	0.77 ± 0.07	0.26 ± 0.06	1.03 ± 0.02	-0.114 ± 0.01	2.91	2.40
2	WT-LAU	14.74 ± 1.13	0.56 ± 0.04	0.53 ± 0.06	1.08 ± 0.01	-0.248 ± 0.01	3.62	2.14
3	WT-PAL	14.52 ± 1.14	0.65 ± 0.05	0.42 ± 0.05	1.06 ± 0.02	-0.121 ± 0.02	3.15	2.35
4	WT-PAL (2UWH coordinates)	14.43 ± 1.18	0.42 ± 0.05	0.64 ± 0.06	1.07 ± 0.02	-0.281 ± 0.01	3.76	2.35
5	WT-MYR	14.28 ± 1.19	0.58 ± 0.05	0.52 ± 0.06	1.09 ± 0.01	-0.214 ± 0.01	3.54	2.35
6	F393A-ACD	14.12 ± 1.05	0.79 ± 0.09	0.30 ± 0.05	1.09 ± 0.01	-0.033 ± 0.01	2.29	2.38
7	F393W-ACD	14.55 ± 1.11	0.54 ± 0.10	0.58 ± 0.04	1.12 ± 0.02	-0.140 ± 0.02	3.09	1.46
8	L86E-ACD	14.43 ± 1.16	0.65 ± 0.11	0.42 ± 0.02	1.07 ± 0.01	-0.162 ± 0.00	3.42	2.33
9	WT-NPG	14.33 ± 1.13	0.60 ± 0.04	0.54 ± 0.05	1.14 ± 0.02	-0.167 ± 0.01	3.41	NA

^{*} ET ΔG° for mutants are scaled to the experimental data for WT BM3.

Table 4. Dependence of the ET reorganization energies λ (protein, solvent contributions; λ_{prot} , λ_{solv}), free energies (ΔG°), cofactor distance (Å) and relative logarithmic ET rates on the square root of the ionic strength (\sqrt{l}).

Sr. No.	Buffer conc.	\sqrt{I}	Cofactor -distance	λ_{prot}	$\lambda_{ m solv}$	ΕΤ λ	ET ΔG°	Cal. log k_{ET}	Exp. log k_{ET}
1	50 mM	0.22	14.66 ± 1.27	0.49 ± 0.06	0.63 ± 0.06	1.13 ± 0.02	0.029 ± 0.01	1.37	1.40
2	250 mM	0.50	14.22 ± 1.19	0.48 ± 0.05	0.62 ± 0.04	1.09 ± 0.02	0.017 ± 0.03	1.94	1.65
3	400 mM	0.63	14.31 ± 1.09	0.60 ± 0.05	0.52 ± 0.08	1.12 ± 0.01	-0.049 ± 0.00	2.18	1.48

The calculated and experimental relative log kET values are w.r.t. the WT BM3 in Table 2. (See supporting information Table S4)

[†] Experimental relative $k_{\rm ET}$ from reference 8 and references cited therein. The calculated and experimental relative log kET values are w.r.t. the WT BM3. (See supporting information Table S4)

[†]Experimental relative $k_{\rm ET}$ are w. r. t. the WT BM3 and calculated from $k_{\rm ET}$ data in references cited therein. NA – data not available in the literature. The calculated and experimental relative log kET values are w.r.t. the WT BM3 in Table 2. (See supporting information Table S4)

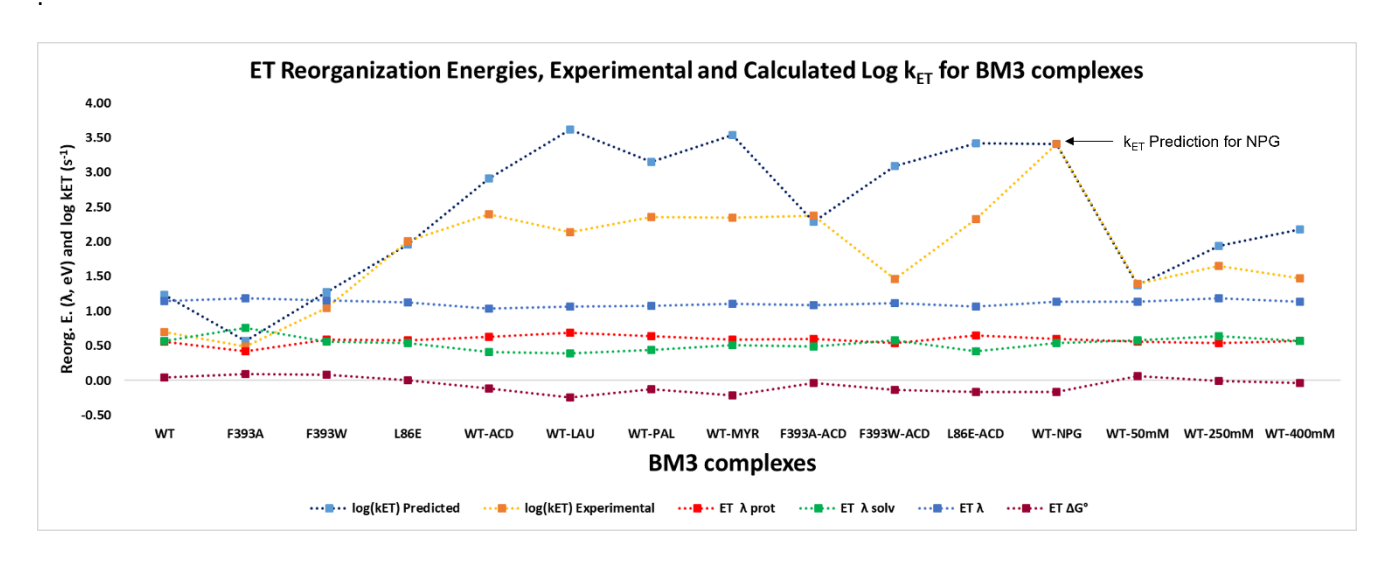


Figure 2. An overview of the electron transfer (ET) total reorganization energies (ET λ), corresponding protein (ET λ_{prot}) and solvent (ET λ_{solv}) contributions, calculated and experimental relative log ET rates; log(k_{ET}) for BM3 wild type (WT), mutants, ligand-bound (WT and mutants), and under three different ion concentrations ([K+] = 50, 250 and 400 mM). ACD; arachidonic acid, LAU; lauric acid, PAL; Palmitic acid, MYR; myristic acid, NPG; N-palmitoyl glycine.

de Beer et al., have calculated the free energy associated with the BM3 catalyzed hydroxylation of alpha-ionone derivatives using thermodynamic integration.53 They invoked Marcus theory to give a qualitative explanation for the correspondence between the reaction-free energy change and the relative rate of product formation. However, this is an oversimplification since Marcus theory applies to only the two outer-sphere ET steps of the CYP450 catalytic cycle and the situation may be more complex as the reaction involves many steps including oxygen binding, two protonations, radical formation, rebound, and product release steps. Thus, free energies (ΔG°) for the first ET step in the CYP450 catalytic cycle have not been measured directly or calculated to date. Although the reorganization energies (λ) for Heme model compounds have been studied in the literature,⁵⁴ the λs for BM3 or any other CYP450s are not known from experiments or calculations (to the best of our knowledge). In the absence of such experimental data, molecular dynamics (MD) simulations have been used for other ET proteins to get reasonably accurate estimates for these important ET parameters. 21,28,29,33,55,56 Such calculations of ET parameters are essential for the estimation of ET rates and have the potential to revolutionize the CYP450 (re)design for various applications mentioned in the introduction. Thus, MD simulations were performed for the LF and LB redox states for the BM3 wild-type and mutants.

Table 2 shows these ET parameters calculated from a triplicate set of MD simulations (see Methods section) namely the average of the minimum distance between Heme and FMN cofactor, ET reorganization energies (λ), free energies (Δ G°), calculated and experimental ET rate ratios. Considering the typical uncertainties associated with ET rates, it is recommended to compare log ET rates. This is a common practice in physical organic chemistry where

instead of trying to make accurate predictions of reaction rates, activation free energies (ΔG^{\ddagger}) or log rates are compared among competing reactions. Considering the accuracy of experimental methods for reaction and activation free energy measurements, calculations within a couple of kcal/mol are considered a good agreement with experiments. Whenever it is necessary to estimate reaction rates it is recommended to report log rates (even for ET proteins), since a difference of only 1.36 kcal/mol in activation free energies leads to a 10-fold difference in calculated rates. Thus, an agreement within one log unit is considered reasonably good. Thus, in this work, log ET rate (log $k_{\rm ET}$) was calculated and compared to the WT BM3.

The ET λ for the WT BM3 and the three F393 and L86 variants are very similar (see Table 2). The F393A mutation lowers the co-factor distance but increases the ET ΔG° . The total ET λ , was decomposed into the respective protein and solvent contributions (λ_{prot} , λ_{solv}) using a procedure reported in the methods section and earlier.³² The conservative nature of the Phe to Trp substitution leads to very similar λ_{prot} , λ_{soly} values. Whereas the non-conservative substitution of Phe with Ala leads to lower and higher protein and solvent λs respectively. For the F393A variant, the variations in these parameters cancel out giving a similar total λ for both proteins (see Figure 2). The conservative mutation (F393W) does not affect the λ_{prot} , and λ_{solv} significantly but it increases the ET ΔG° and lowers the co-factor distance. The ET rates for this variant have been reported to be moderately higher than the WT and the F393A variant. The calculated $\log k_{\rm ET}$ for the non-conservative mutant (F393A) is lower than the F393W variant in agreement with the experimental data.8,50 For the non-conservative mutation L86E, the total and individual λ contributions remain very similar to WT, but the calculated ET ΔG° is zero. This seemed counterintuitive since the additional negative charge introduced by this mutation should decrease the stability of the ferrous state. An analysis of MD trajectories showed the presence of bridging water molecules between the Heme and Glu residue in approximately half of the snapshots (1054) thus rationalizing the stabilization of the reduced Ferrous state despite the presence of negatively charged Glu residue near the Heme centre. This in combination with smaller cofactor distance increases the calculated $\log k_{\rm ET}$ values in agreement with experimental trends. These log $k_{\rm ET}$ values are in correspondence with the experimental data for the ligand-free (LF) proteins (see Table 2). Thus, the current methodology predicts the trends in ET rates in LF BM3 variants and was used for the prediction of the influence of ligand binding on the WT protein and corresponding variants (discussed in the next section).

Influence of ligand binding on ET parameters and rates

As mentioned earlier natural substrates (ligands) of BM3, free fatty acids (ACD, PAL, LAU, and MYR), have been studied extensively and $k_{\rm ET}$ for these ligand-BM3 complexes are known in the literature. However, a molecular-level understanding of these rates in terms of ET parameters is missing. Table 3 shows the calculated ET parameters and log ET rates for the LB WT BM3 and variants considered in this study. Ligand binding reduces the ET ΔG° (driving force) required for the ET and the total ET λ for most of the complexes by 0.07-0.29 V and \sim 0.1 eV respectively, thus giving enhanced ET upon binding. The finding that mutations have a smaller influence on the ET ΔG° , and λ compared to ligands is in excellent agreement with literature reports on different mutants and ligand studies.8 The differences in the interactions between the ligands and BM3 are manifested in their respective ET ΔG°, and protein, and solvent reorganization energies (λ_{prot} , λ_{solv}) which also modulate the log k_{ET} (see Figure 2 and Table 3). ACD binding lowers ET ΔG° by 0.153 V in excellent agreement with the experimental data

 $0.129~V.^{8}~$ The λ_{solv} is also lowered (by ACD binding) which compensates for a higher λ_{prot} and cofactor distance thus increased $\log k_{\rm ET}$ are predicted in concordance with the experiments. For PAL binding the reduction in the ET ΔG° is also in close agreement with experimental data (0.160 V). Using the PAL crystal structure coordinates (2UWH) for ET parameter and rate calculations gives a lower co-factor distance (0.1 Å), higher ET ΔG° , and compensatory changes in λ_{prot} , λ_{solv} leading to $\log k_{\text{ET}}$ within 1 \log unit of that estimated with the docking pose. This further validates our methodology for ET parameter and rate calculations. MYR and PAL bring the two cofactors closer compared to LAU, thus exhibiting an increase in $\log k_{\rm ET}$ despite higher $\lambda_{\rm solv}$. LAU has a larger influence on all these parameters giving a higher log $k_{\rm ET}$ than LF BM3. The difference in the calculated and experimental $\log k_{\rm ET}$ for LAU-bound WT BM3 is more than one \log unit. Since, the experimental ET ΔG° and the co-factor distance (crystal structure) for this ligand are unknown, both these factors might contribute to this discrepancy. Thus overall, our methodology for ET parameter and log $k_{\rm ET}$ calculations reproduces the order in agreement with experimental trends compared to the WT BM3. N-palmitoyl glycine (NPG) is a known substrate of BM3, but the rate for the first ET between Heme and FMN domains is not reported in the literature. Shaikh et al., have predicted a range of ET rates (6 to 235 s-1) based on co-factor distances derived from MD simulation.²⁵ This gives a wide range for the log $k_{\rm ET}$ between 1 to 2.37. As mentioned in the introduction they did not explicitly calculate the ET λ or ΔG° values but instead used Dutton's empirical model.60 In our calculations, NPG induces a reduction in ET ΔG° comparable to other ligands and shows marginally higher (λ_{prot} , λ_{solv}) which are compensated by marginally smaller co-factor distance. This gives an estimate of relative $\log k_{\rm ET}$ rate comparable to other ligands and in accord with literature understanding on the effect of ligands.

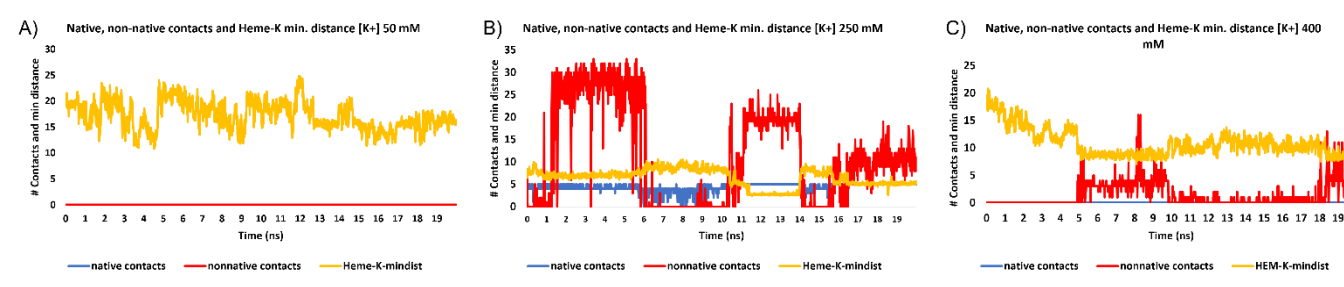


Figure 3. The number of Heme cofactor and K+ ion native and non-native contacts (blue and red) and minimum distance (orange) in the Heme reduced (Fe2) and FMN oxidized (FMN-ox) state during the 20 ns MD simulation. For the simulations with A) 50 mM, B) 250 mM and C) 400 mM ion concentration.

Considering the interest in the BM3 mutants for biotechnological applications, we decided to test our methodology for the variants with known $k_{\rm ET}$ for ACD-bound complexes. The F393A mutation gives a smaller reduction in ET ΔG° (0.07 V) and marginally affects the $\lambda_{\rm prot}$, $\lambda_{\rm solv}$, and total λ , but the smaller cofactor distance compensates for higher reorganization energies and thus has a log $k_{\rm ET}$ = 2.29. This is similar to the experimental log $k_{\rm ET}$ = 2.38. The ACD binding to the F393W mutant recovers the lowering of ET ΔG° (driving force) and shows $\lambda_{\rm prot}$, and $\lambda_{\rm solv}$ like the WT BM3. This

compensates for a marginally larger cofactor distance leading to an increase in the log $k_{\rm ET}$ to 3.09. This value is higher than the experimental log $k_{\rm ET}$, and can be traced to the higher total λ and ET Δ G°. Nonetheless, the influence of ligand binding and experiment trend (important for protein engineers) compared to the WT LF BM3 is captured. The ACD binding to the L86E variant also recovers the ET Δ G°. It shows a considerably lower $\lambda_{\rm solv}$ and marginally lower cofactor distance, thus giving a log $k_{\rm ET}$ = 3.42 in correspondence with the experimental trend compared to the WT LF

BM3 and is within one log unit with respect to the WT LB BM3. Thus overall our predictions agree with the experimental trends in log $k_{\rm ET}$ (see Table 3 and Figure 2) and establish the predictive value of our methodology for analyzing the relative influence of mutations and ligands on the ET parameters and rates for WT BM3.

Influence of ionic strength on ET parameters and rates

The relationship between the ionic strength and ET rates $(k_{\rm ET})$ in redox proteins is complex and depends on the nature of interactions with ET partners. The dominant binding mechanism between the two proteins can be electrostatic or mixed electrostatic/H-bonding/hydrophobic.61-64 Nonetheless, often the reported $k_{\rm ET}$ values show a bellshaped (or inverted bell-shaped) dependence against the ionic strength for CYP450s.14,61 Gillardi et al., found that ET between FMN and Heme domains of BM3 show bell-shaped dependence on the ionic strength of the solution.¹⁴ ET rates increased marginally from a value of 25 s⁻¹ at 50 mM to 45 s-1 at 250 mM but then decreased back to 30 s-1 at 400 mM (see reference 14). Since these variations in $k_{\rm ET}$ are small, it serves as a challenging case for the proposed methodology to model the influence of ionic strength on ET parameters and rates in BM3. SLTCAP method was used to calculate the number of K+ and counter ions required in the MD simulation box to achieve the desired ion concentration (see Table 4 and Table S2).65

Table 4 shows the dependence of cofactor distance, ET parameters, and log ET rates on the square root of the ionic strength (\sqrt{I}). At moderate ionic strength (ion concentration = 250 mM), the total λ decreases marginally (1.09 eV). This agrees with older findings for other ET proteins e.g., Ru-65-CytB5 system.⁶⁴ The higher ionic strength has a larger influence on the individual λ_{prot} and λ_{solv} contributions. The cofactor distance is marginally lower at the intermediate ionic strength (entry 2 Table 4). An increase in the ionic concentration predicts an increasing ET ΔG° . This coupled with a smaller cofactor distance for intermediate ionic strength (250 mM) leads to an increase in the log $k_{\rm ET}$. The $\log k_{\mathrm{ET}}$ for higher ionic strength is in close agreement with the experimental data but still is slightly off for the expected trend when compared with lower ionic strength experimental data (Table 4). The use of a non-polarizable force field and ion parameters could cause less than perfect agreement with experimental results which have smaller variations compared to the influence of mutations and ligand binding.^{66,67} Thus, considering the uncertainty in the experimental ET rates, these results can be considered preliminary and should be confirmed in the future with additional experiments and simulations. Overall, the calculated $\log k_{\rm ET}$ and experimental $\log k_{\rm ET}$ across mutants, ligand bound-states, and with ions show a good correlation (r^2 = 0.68, see Figure S6).

QM calculations on model systems have shown earlier that the reduced (Ferrous) state stabilization by monovalent alkali metal ions is effective up to 10 $\rm \AA.^{16}$ Thus the MD trajectories for these ion concentrations were analyzed for

Heme-K contacts. Figure 3 shows the number of K⁺ ions in close contact (< 10 Å) with the Heme cofactor and the minimum distance at which these ions approach the Heme. At lower ionic strengths (see panel A of Figure 3), the K⁺ ions move between 15-25 Å from the Heme, rarely approaching any closer, thus the number of contacts within 10 Å remains zero. Similarly at much higher ionic strength, $[K^+] = 400$ mM, the minimum distance barely approaches 10 Å and the number of contacts remains relatively spare (see panel C of Figure 3). In contrast, at intermediate ion strength, $[K^+]$ = 250 mM, the minimum distance between the ion and the Heme cofactor is substantially smaller and remains between 5-10 Å for most of the time during the 20 ns MD simulation. As a result, the number of contacts between the Heme atoms and K⁺ ion is substantially higher (see panel B of Figure 3). These observations also agree with the number of contacts between K+ and protein residues at different concentrations analyzed by the nativecontacts command in cpptraj.68 At 50 mM, an average of 5.3 ± 3.1 K+ ions come within 3.0 Å of BMP (Heme domain) residues (see Table S3). At intermediate concentrations (250 mM) the average number of contacts between K+ and BMP residues increases to 10.7 ± 1.2. Whereas at 400 mM this value decreases back to 5.0 ± 2.0 . This taken together with observations in Figure 3, shows that at moderate K+ ion concentrations (250 mM) larger number of K⁺ ions come in close contact with the protein atoms, thus contributing to the stabilization of extra electronic charge transferred from the BMR (FMN). This coupled with our earlier work on model systems. 16 provides convincing evidence for the mechanism for the modulation of the ET rates by the positively charged K⁺ ions (namely the stabilization of the reduced Ferrous state of BM3).

CONCLUSIONS

An MD simulation-based methodology (called CYPWare 1.0) was developed to calculate the electron transfer (ET) parameters and rates for the CYP450 BM3 wild type (WT) and mutants. CYPWare 1.0, automates all the MD simulations on docked poses for ET parameter extraction and analysis steps. Initially, vina docking correctly placed the sites of metabolism (SOMs) of typical fatty acid substrates in close vicinity of the Heme Fe and the predicted binding affinities followed experimental trends. MD simulations of two redox states facilitate calculations of the vertical energy gaps ($\Delta E_{a,b}$) and ET reorganization and free energies (λ and ΔG°) for the BM3 WT which are similar to those reported earlier for other Heme redox proteins. The average cofactor distances measured in MD simulations for the ligand-free (LF) states are smaller than the earlier reports for the Heme oxidized state alone.²⁵ Nonetheless, our ET rate calculations using semi-classical Marcus theory are in good agreement with the experimental data. This suggests that the variations in the cofactor (FMN to Heme) distance upon ligand binding are smaller than predicted earlier. Thus, we established that the BM3 ET ΔG° , calculated explicitly for the first time, plays an important role in determining the BM3 ET rates. Decomposition of the total ET λ into the protein and solvent contributions (λ_{prot} , λ_{solv}) combined with ET ΔG° explains the influence of mutation on ET rates. Ligand binding does not affect the total ET λs , rather it influences relative λ_{prot} , λ_{solv} contributions, and ET ΔG° . Ligands (ACD, PAL, MYR), that lower the λ_{solv} , and increase the ET driving force (lowering the ET ΔG°) lead to ET rate enhancements.

BM3 mutations with increased ET rates in the LF state mostly act by lowering the cofactor distances and increasing the ET driving force (lowering ΔG°). For LB BM3 mutants (F393A), a lowering of both the λ_{solv} contributions, ET ΔG° , and average cofactor distances contribute to ET rate enhancements. Whereas LB mutants (F393W) that do not reduce the ET parameters (λ and cofactor distance) display lower ET rate enhancements upon ligand binding despite lowering the ET ΔG° . Our methodology also captures the effect of low and moderate ionic strength (concentrations) on ET parameters and rates. At moderate ionic strength (\sqrt{l} = 0.50) the cofactor distance and ET ΔG° are lowered and a larger number of K+ ions approach the Heme domain leading to moderate enhancements in ET rates.

In summary, our MD simulation-based methodology effectively captures the major influences of mutations, ligand binding, and changes in ionic strength on the ET parameters and rates in BM3 and its variants. This methodology is directly applicable to all CYP450 redox systems with only one requirement of a known experimental ET driving force for at least one variant or WT protein complex. For other redox enzymes an additional initial step involving parameterization for associated co-factors with MCBP.py tool will be necessary. All the MD simulations (360 ns/variant), energy calculations, and analysis require 6 hours on GPU enabled HPC. CYPWare 1.0, script and the web tool used to define input variables are available on GitHub. The methodology is being integrated with standard directed evolution modeling methods to identify ET rate-enhancing mutations and will be communicated soon elsewhere.

ASSOCIATED CONTENT

Supporting Information.

The supporting information file contains: 1) Modeller and tleap scripts to generate linker coordinates, 2) Figures S1 and S2 showing linker positions and comparison of docked and crystal structure poses for NPG, 3) PAL and Heme contact analysis, 4) Figure S3 and S4 show PAL and ACD omega carbon atom distances from Heme-Fe respectively, 5) Table S1 and Figure S5 docking scores and correlation, 6) Table S2 shows number of ions calculated with SLTCAP method, 7) Figure S6 shows the scatter plot between experimental and calculated log $k_{\rm ET}$. 8) Figure S7 and S8 shows PAL omega carbon atom distances from Heme Fe for the oxidized and the reduced states, 9) Table S3 shows the total number of K+ ions within 3 Å of the BM3 protein and BMP (Heme domain) for different ion concentrations. 10) Figure S9-S13 RMSD plots for LF and LB BM3 complexes.

AUTHOR INFORMATION

Corresponding Author

* Vaibhav A. Dixit (vaibhavadixit@gmail.com, and vaibhav@niperguwahati.in).

Author Contributions

VAD conceptualized and managed the work, wrote the funding proposal, performed simulations, and analysis, wrote the CYP-Ware 1.0 program, wrote the manuscript, and participated in email/online discussions. USN M and PB participated in discussions. JB and SdeV participated in discussions, and manuscript writing and gave expert advice in data analysis. All authors have given approval to the final version of the manuscript.

Funding Sources

VAD acknowledges the financial support from the National Supercomputing Mission (NSM), Department of Science and Technology (DST), New Delhi (Ref. No. DST/NSM/R&D_HPC_Applications/2021/09).

Notes

ACKNOWLEDGMENT

Computational resources for this work were provided by the National Institute of Pharmaceutical Education and Research, Guwahati (NIPER-G), and PARAM Shivay Facility under the National Supercomputing Mission, Government of India at the Indian Institute of Technology, Varanasi is also gratefully acknowledged. Reference number: DST/NSM/R&D_HPC_Applications/2021/09. The authors are thankful to the C-DAC, Pune team for developing the web tool (Mr. Saurabh G., Mr. Nikhil R., Dr. Rajendra Joshi).

Data and Software Availability

The protein and ligand structures used in this work are available publicly in Protein Data Bank and PubChem. Modeller and tleap scripts are provided in the supporting information. CYPWare 1.0 program and the web tool are free for academic research and are available on the GitHub repository of the PI (https://github.com/Dixit-s-lab/CYPWare-1.0). Details on the installation and usage are available on the repository readme page. CYPWare 1.0 utilizes open-source tools like obabel, AmberTools20, and AmberMdPrep, cpptraj and statistical tool (st) which are available on respective GitHub repositories. Amber20 is available from UCSF at discounted rates for academic research.

ABBREVIATIONS

CYP450, cytochrome P450;; ET, electron transfer, MD, molecular dynamics.

REFERENCES

(1) Sawayama, A. M.; Chen, M. M. Y.; Kulanthaivel, P.; Kuo, M. S.; Hemmerle, H.; Arnold, F. H. A Panel of Cytochrome P450 BM3 Variants to Produce Drug Metabolites and Diversify Lead Compounds. *Chemistry*– A European Journal 2009, 15 (43), 11723–11729.

https://doi.org/10.1002/CHEM.200900643

11

- di Nardo, G.; Gilardi, G. Optimization of the Bacterial Cytochrome P450 BM3 System for the Production of Human Drug Metabolites. *Int J Mol Sci* **2012**, *13* (12), 15901–15924. https://doi.org/10.3390/IJMS131215901.
- (3) Reinen, J.; van Leeuwen, J. S.; Li, Y.; Sun, L.; Grootenhuis, P. D. J.; Decker, C. J.; Saunders, J.; Vermeulen, N. P. E.; Commandeur, J. N. M. Efficient Screening of Cytochrome P450 BM3 Mutants for Their Metabolic Activity and Diversity toward a Wide Set of Drug-Like Molecules in Chemical Space. *Drug Metabolism and Disposition* 2011, 39 (9), 1568–1576. https://doi.org/10.1124/DMD.111.039461.
- (4) Butler, C. F.; Peet, C.; Mason, A. E.; Voice, M. W.; Leys, D.; Munro, A. W. Key Mutations Alter the Cytochrome P450 BM3 Conformational Landscape and Remove Inherent Substrate Bias. *Journal of Biological Chemistry* **2013**, *288* (35), 25387–25399. https://doi.org/10.1074/JBC.M113.479717 /ATTACHMENT/D0786469-0E8E-4CAD-9518-6E367BEA-BECA/MMC1.PDF.
- (5) Kanoh, N.; Kawamata-Asano, A.; Suzuki, K.; Takahashi, Y.; Miyazawa, T.; Nakamura, T.; Moriya, T.; Hirano, H.; Osada, H.; Iwabuchi, Y.; Takahashi, S. An Integrated Screening System for the Selection of Exemplary Substrates for Natural and Engineered Cytochrome P450s. *Sci Rep* 2019, 9 (1), 1–13. https://doi.org/10.1038/s41598-019-54473-8.
- (6) Voskarides, K. Directed Evolution. The Legacy of a Nobel Prize. *Journal of Molecular Evolution*. Springer November 13, 2020, pp 1–3. https://doi.org/10.1007/s00239-020-09972-y.
- (7) Arnold, F. H. Directed Evolution: Bringing New Chemistry to Life. *Angewandte Chemie International Edition* **2018**, *57*

- (16), 4143–4148. https://doi.org/10.1002/anie.201708408.
- (8) C. Whitehouse, C. J.; G. Bell, S.; Luet-Lok Wong. P450 BM3 (CYP102A1): Connecting the Dots. *Chem Soc Rev* **2012**, *41* (3), 1218–1260. https://doi.org/10.1039/C1CS15192D.
- (9) Dubey, K. D.; Wang, B.; Shaik, S. Molecular Dynamics and QM/MM Calculations Predict the Substrate-Induced Gating of Cytochrome P450 BM3 and the Regio- and Stereoselectivity of Fatty Acid Hydroxylation. *J Am Chem Soc* **2016**, *138* (3), 837–845. https://doi.org/10.1021/jacs.5b08737.
- (10) Capoferri, L.; Leth, R.; ter Haar, E.; Mohanty, A. K.; Grootenhuis, P. D. J.; Vottero, E.; Commandeur, J. N. M.; Vermeulen, N. P. E.; Jørgensen, F. S.; Olsen, L.; Geerke, D. P. Insights into Regioselective Metabolism of Mefenamic Acid by Cytochrome P450 BM3 Mutants through Crystallography, Docking, Molecular Dynamics, and Free Energy Calculations. *Proteins: Structure, Function, and Bioinformatics* **2016**, 84 (3), 383–396. https://doi.org/10.1002/PROT.24985.
- (11) Kirchmair, J.; Mannhold, R. *Drug Metabolism Prediction, Volume 63*; WILEY-VCH Verlag GmbH, Weinheim: Zurich, 2014; Vol. 63.
- (12) Dixit, V. A.; Lal, L. A.; Agrawal, S. R. Recent Advances in the Prediction of Non-CYP450-Mediated Drug Metabolism. Wiley Interdiscip Rev Comput Mol Sci 2017, 7 (6), e1323. https://doi.org/10.1002/wcms.1323.
- (13) Dixit, V. A.; Deshpande, S. Advances in Computational Prediction of Regioselective and Isoform-Specific Drug Metabolism Catalyzed by CYP450s. *ChemistrySelect*. December 1, 2016, pp 6571–6597. https://doi.org/10.1002/slct.201601051.

- (14) Gilardi, G.; Meharenna, Y. T.; Tsotsou, G. E.; Sadeghi, S. J.; Fairhead, M.; Giannini, S. Molecular Lego: Design of Molecular Assemblies of P450 Enzymes for Nanobiotechnology. *Biosens Bioelectron* **2002**, *17* (1–2), 133–145. https://doi.org/10.1016/S0956-5663(01)00286-X.
- (15) Gemzik, B.; Halvorson, M. R.; Parkinson, A. Pronounced and Differential Effects of Ionic Strength and PH on Testosterone Oxidation by Membrane-Bound and Purified Forms of Rat Liver Microsomal Cytochrome P-450. *J Steroid Biochem* **1990**, *35* (3–4), 429–440. https://doi.org/10.1016/0022-4731(90)90251-M.
- (16) Dixit, V. A.; Warwicker, J.; de Visser, S. P. How Do Metal Ions Modulate the Rate-Determining Electron-Transfer Step in Cytochrome P450 Reactions? *Chemistry A European Journal* **2020**, *26* (66), 15270–15281. https://doi.org/10.1002/chem.202003024.
- (17) Tipmanee, V.; Oberhofer, H.; Park, M.; Kim, K. S.; Blumberger, J. Prediction of Reorganization Free Energies for Biological Electron Transfer: A Comparative Study of Ru-Modified Cytochromes and a 4-Helix Bundle Protein. *J Am Chem Soc* **2010**, *132* (47), 17032–17040. https://doi.org/10.1021/ja107876p.
- (18) Chen, M. M.; Coelho, P. S.; Arnold, F. H. Utilizing Terminal Oxidants to Achieve P450-Catalyzed Oxidation of Methane. *Adv Synth Catal* **2012**, *354* (6), 964–968. https://doi.org/10.1002/adsc.201100833.
- (19) Llanos, M. A.; Gantner, M. E.; Rodriguez, S.; Alberca, L. N.; Bellera, C. L.; Talevi, A.; Gavernet, L. Strengths and Weaknesses of Docking Simulations in the SARS-CoV-2 Era: The Main Protease (Mpro) Case Study. *J Chem Inf Model* **2021**, *61* (8), 3758–3770. https://doi.org/10.1021/ACS.JCIM.1C004

- 04/SUPPL_FILE/CI1C00404_SI_003.XL SX.
- (20) Abagyan, R.; Rueda, M.; Bottegoni, G. Recipes for the Selection of Experimental Protein Conformations for Virtual Screening. *J Chem Inf Model* **2010**, *50* (1), 186–193. https://doi.org/10.1021/CI9003943/SUPPL_FILE/CI9003943_SI_001.PDF.
- (21) Tipmanee, V.; Oberhofer, H.; Park, M.; Kim, K. S.; Blumberger, J. Prediction of Reorganization Free Energies for Biological Electron Transfer: A Comparative Study of Ru-Modified Cytochromes and a 4-Helix Bundle Protein. *J Am Chem Soc* **2010**, *132* (47), 17032–17040. https://doi.org/10.1021/ja107876p.
- (22) Foloppe, N.; Chen, I.-J. The Reorganization Energy of Compounds upon Binding to Proteins, from Dynamic and Solvated Bound and Unbound States. *Bioorg Med Chem* **2021**, *51*, 116464. https://doi.org/10.1016/J.BMC.2021.11646 4.
- (23) Foloppe, N.; Chen, I.-J. Towards Understanding the Unbound State of Drug Compounds: Implications for the Intramolecular Reorganization Energy upon Binding. *Bioorg Med Chem* **2016**, *24* (10), 2159–2189. https://doi.org/10.1016/J.BMC.2016.03.02 2.
- (24) Samir Chattopadhyay; Manjistha Mukherjee; Banu Kandemir; Bowman, S.; L Bren, K.; Abhishek Dey. Contributions to Cytochrome c Inner- and Outer-Sphere Reorganization Energy. *Chem Sci* **2021**, *12*, 11894–11913. https://doi.org/10.1039/D1SC02865K.
- (25) Dubey, K. D.; Shaik, S. Choreography of the Reductase and P450BM3 Domains Toward Electron Transfer Is Instigated by the Substrate. *J Am Chem Soc* **2018**, *140* (2),

- 683–690. https://doi.org/10.1021/jacs.7b10072.
- (26) Humphrey, W.; Dalke, A.; Schulten, K. VMD: Visual Molecular Dynamics. *J Mol Graph* **1996**, *14* (1), 33–38. https://doi.org/10.1016/0263-7855(96)00018-5.
- (27) Verma, R.; Schwaneberg, U.; Roccatano, D. Insight into the Redox Partner Interaction Mechanism in Cytochrome P450BM-3 Using Molecular Dynamics Simulations. *Biopolymers* **2014**, *101* (3), 197–209. https://doi.org/10.1002/BIP.22301.
- (28) Jiang, X.; Burger, B.; Gajdos, F.; Bortolotti, C.; Futera, Z.; Breuer, M.; Blumberger, J. Kinetics of Trifurcated Electron Flow in the Decaheme Bacterial Proteins MtrC and MtrF. *Proc Natl Acad Sci U S A* **2019**, *116* (9), 3425–3430. https://doi.org/10.1073/pnas.1818003116.
- (29) Jiang, X.; van Wonderen, J. H.; Butt, J. N.; Edwards, M. J.; Clarke, T. A.; Blumberger, J. Which Multi-Heme Protein Complex Transfers Electrons More Efficiently? Comparing MtrCAB from Shewanella with OmcS from Geobacter. *Journal of Physical Chemistry Letters* **2020**, *11*, 9421–9425. https://doi.org/10.1021/acs.jpclett.0c02842
- (30) Jiang, X.; Futera, Z.; Ali, M. E.; Gajdos, F.; von Rudorff, G. F.; Carof, A.; Breuer, M.; Blumberger, J. Cysteine Linkages Accelerate Electron Flow through Tetra-Heme Protein STC. *J Am Chem Soc* **2017**, *139* (48), 17237–17240. https://doi.org/10.1021/jacs.7b08831.
- (31) Breuer, M.; Zarzycki, P.; Shi, L.; Clarke, T. A.; Edwards, M. J.; Butt, J. N.; Richardson, D. J.; Fredrickson, J. K.; Zachara, J. M.; Blumberger, J.; Rosso, K. M. Molecular Structure and Free Energy Landscape for Electron Transport in the Decahaem Cytochrome MtrF. In *Biochemical Society Transactions*; Portland Press, 2012; Vol.

- 40, pp 1198–1203. https://doi.org/10.1042/BST20120139.
- (32) Dixit, V. A.; Blumberger, J.; Vyas, S. K. Methemoglobin Formation in Mutant Hemoglobin α Chains: Electron Transfer Parameters and Rates. *Biophys J* 2021, *120* (17), 3807–3819. https://doi.org/10.1016/j.bpj.2021.07.007.
- (33) Blumberger, J. Recent Advances in the Theory and Molecular Simulation of Biological Electron Transfer Reactions. *Chem Rev* **2015**, *115* (20), 11191–11238. https://doi.org/10.1021/acs.chemrev.5b002 98.
- (34) Laidler, K. Chemical Kinetics, 3rd Edition | Pearson.
- (35) RCSB PDB 1BVY: COMPLEX OF THE HEME AND FMN-BINDING DOMAINS OF THE CYTOCHROME P450(BM-3). https://www.rcsb.org/structure/1BVY (accessed 2021-12-18).
- (36) Fiser, A.; Kinh, R.; Do, G.; Ali, A. S. *. Modeling of Loops in Protein Structures. *Protein Science* **2000**, *9* (9), 1753–1773. https://doi.org/10.1110/PS.9.9.1753.
- (37) Fiser, A.; Sali, A. ModLoop: Automated Modeling of Loops in Protein Structures. *Bioinformatics* **2003**, *19* (18), 2500–2501. https://doi.org/10.1093/BIOINFORMAT-ICS/BTG362.
- (38) Anandakrishnan, R.; Aguilar, B.; Onufriev, A. v. H++ 3.0: Automating PK Prediction and the Preparation of Biomolecular Structures for Atomistic Molecular Modeling and Simulations. *Nucleic Acids Res* **2012**, 40 (W1), W537–W541. https://doi.org/10.1093/nar/gks375.
- (39) H++ (web-based computational prediction of protonation states and pK of ionizable groups in macromolecules). http://biophysics.cs.vt.edu/ (accessed 2021-01-05).

- (40) Li, P.; Merz, K. M. MCPB.Py: A Python Based Metal Center Parameter Builder. J Chem Inf Model 2016, 56 (4), 599–604. https://doi.org/10.1021/acs.jcim.5b00674.
- (41) Frisch, M. J.; Trucks, G. W.; Schlegel, H. B.; Scuseria, G. E.; Robb, M. A.; Cheeseman, J. R.; Scalmani, G.; Barone, V.; Mennucci, B.; Petersson, G. A.; Nakatsuji, H.; Fox, D. J.; et al. Gaussian 09 Revision C.01. Gaussian, Inc., Wallingford CT.
- Pengfei, L.; Kenneth, M. M. Jr. Building Bonded Model for A HEME Group with MCPB.py. Amber20 Tutorial. http://ambermd.org/tutorials/advanced/tutorial20/mcpbpy heme.htm (accessed 2021-12-20).
- (43) Case, D. A.; Aktulga, H. M.; Belfon, K.; Ben-Shalom, I. Y .; Brozell, S. R.; Cerutti, D. S.; Cheatham III, T. E.; Cisneros, G. A.; Cruzeiro, V. W. D.; Darden, T. A.; et al. Amber 2021; University of California Press, 2021.
- O'Boyle, N. M.; Banck, M.; James, C. A.; Morley, C.; Vandermeersch, T.; Hutchison, G. R. Open Babel: An Open Chemical Toolbox. J Cheminform 2011, 3 (1), 33. https://doi.org/10.1186/1758-2946-3-33.
- Trott, O.; Olson, A. J. AutoDock Vina: Im-(45)proving the Speed and Accuracy of Docking with a New Scoring Function, Efficient Optimization, and Multithreading. J Comput Chem **2009**, 31 (2), 455–461. https://doi.org/10.1002/jcc.21334.
- Roe, D. R.; Brooks, B. R. A Protocol for (46)Preparing Explicitly Solvated Systems for Stable Molecular Dynamics Simulations. Journal of Chemical Physics 2020, 153 (5), 054123. https://doi.org/10.1063/5.0013849.
- Stein, R. M.; Yang, Y.; Balius, T. E.; (47) O'Meara, M. J.; Lyu, J.; Young, J.; Tang, K.; Shoichet, B. K.; Irwin, J. J. Property-

- Unmatched Decoys in Docking Benchmarks. J Chem Inf Model 2021, 61 (2), 699-714. https://doi.org/10.1021/ACS.JCIM.0C005 98/SUPPL FILE/CI0C00598 SI 009.XL SX.
- Chen, H.; Lyne, P. D.; Giordanetto, F.; (48)Lovell, T.; Li, J. On Evaluating Molecular-Docking Methods for Pose Prediction and Enrichment Factors. J Chem Inf Model 2005, 46 (1),401–415. https://doi.org/10.1021/CI0503255.
- (49)Butler, C. F.; Peet, C.; Mason, A. E.; Voice, M. W.; Leys, D.; Munro, A. W. Key Mutations Alter the Cytochrome P450 BM3 Conformational Landscape and Remove Inherent Substrate Bias. Journal of Biological Chemistry 2013, 288 (35), 25387–25399. https://doi.org/10.1074/JBC.M113.479717 /ATTACHMENT/D0786469-0E8E-4CAD-9518-6E367BEA-BECA/MMC1.PDF.
- (50)Ost, T. W. B.; Clark, J.; Mowat, C. G.; Miles, C. S.; Walkinshaw, M. D.; Reid, G. A.; Chapman, S. K.; Daff, S. Oxygen Activation and Electron Transfer in Flavocytochrome P450 BM3. J Am Chem Soc 2003, 125 (49),15010-15020. https://doi.org/10.1021/JA035731O.
- Fleming, B. D.; Tian, Y.; Bell, S. G.; Wong, (51)L.-L.; Urlacher, V.; Hill, H. A. O. Redox Properties of Cytochrome P450BM3 Measured by Direct Methods. Eur J Bio-2003. 270 (20),4082–4088. https://doi.org/10.1046/J.1432-1033.2003.03799.X.
- (52)Sevrioukova, I. F.; Li, H.; Zhang, H.; Peterson, J. A.; Poulos, T. L. Structure of a Cytochrome P450-Redox Partner Electron-Transfer Complex. Proceedings of the National Academy of Sciences 1999, 96 (5), 1863-1868.
 - https://doi.org/10.1073/PNAS.96.5.1863.

- (53) Beer, S. B. A. de; Venkataraman, H.; Geerke, D. P.; Oostenbrink, C.; Vermeulen, N. P. E. Free Energy Calculations Give Insight into the Stereoselective Hydroxylation of α-Ionones by Engineered Cytochrome P450 BM3 Mutants. *J Chem Inf Model* **2012**, *52* (8), 2139–2148. https://doi.org/10.1021/CI300243N.
- (54) Bandyopadhyay, S.; Rana, A.; Mittra, K.; Samanta, S.; Sengupta, K.; Dey, A. Effect of Axial Ligand, Spin State, and Hydrogen Bonding on the Inner-Sphere Reorganization Energies of Functional Models of Cytochrome P450. *Inorg Chem* **2014**, *53* (19), 10150–10158. https://doi.org/10.1021/IC501112A/SUPP L_FILE/IC501112A_SI_001.PDF.
- (55) Simonneaux, G.; Bondon, A. Mechanism of Electron Transfer in Heme Proteins and Models: The NMR Approach. *Chem Rev* **2005**, 105 (6), 2627–2646. https://doi.org/10.1021/cr030731s.
- (56) Blumberger, J. Free Energies for Biological Electron Transfer from QM/MM Calculation: Method, Application and Critical Assessment. *Physical Chemistry Chemical Physics* **2008**, *10* (37), 5651–5667. https://doi.org/10.1039/b807444e.
- Yang, T.; Quesne, M. G.; Neu, H. M.; Reinhard, F. G. C.; Goldberg, D. P.; de Visser, S. P. Singlet versus Triplet Reactivity in an Mn(V)-Oxo Species: Testing Theoretical Predictions Against Experimental Evidence. *J Am Chem Soc* 2016, *138* (38), 12375–12386.
 https://doi.org/10.1021/JACS.6B05027/SU PPL FILE/JA6B05027 SI 001.PDF.
- (58) Cantu Reinhard, F. G.; Faponle, A. S.; de Visser, S. P. Substrate Sulfoxidation by an Iron(IV)-Oxo Complex: Benchmarking Computationally Calculated Barrier Heights to Experiment. *Journal of Physical Chemistry A* **2016**, *120* (49), 9805–9814. https://doi.org/10.1021/ACS.JPCA.6B097

- $65/SUPPL_FILE/JP6B09765_SI_001.PDF$.
- (59) Cantú Reinhard, F. G.; Sainna, M. A.; Upadhyay, P.; Balan, G. A.; Kumar, D.; Fornarini, S.; Crestoni, M. E.; de Visser, S. P. A Systematic Account on Aromatic Hydroxylation by a Cytochrome P450 Model Compound I: A Low-Pressure Mass Spectrometry and Computational Study. *Chemistry – A European Journal* 2016, 22 (51), 18608–18619. https://doi.org/10.1002/CHEM.201604361
- (60) Page, C. C.; Moser, C. C.; Chen, X.; Dutton, P. L. Natural Engineering Principles of Electron Tunnelling in Biological Oxidation-Reduction. *Nature* **1999**, *402* (6757), 47–52. https://doi.org/10.1038/46972.
- (61) Voznesensky, A. I.; Schenkman, J. B. The Cytochrome P450 2B4-NADPH Cytochrome P450 Reductase Electron Transfer Complex Is Not Formed by Charge-Pairing. *Journal of Biological Chemistry* **1992**, *267* (21), 14669–14676. https://doi.org/10.1016/S0021-9258(18)42093-5.
- (62) Karlsson, J. J.; Rostrup, T. E.; Ulstrup, J. PH and Ionic Strength Effects on Electron Transfer Rate Constants and Reduction Potentials of the Bacterial Di-Heme Protein Pseudomonas Stutzeri Cytochrome C4. *Acta Chem Scand* **1996**, *50* (3), 284–288. https://doi.org/10.3891/ACTA.CHEM.SC AND.50-0284.
- (63) Yue, H.; Waldeck, D. H.; Petrović, J.; Clark, R. A. The Effect of Ionic Strength on the Electron-Transfer Rate of Surface Immobilized Cytochrome c. *Journal of Physical Chemistry B* **2006**, *110* (10), 5062–5072. https://doi.org/10.1021/JP055768Q.
- (64) Scott, J. R.; McLean, M.; Sligar, S. G.; Durham, B.; Millett, F. Effect of Binding Cytochrome c and Ionic Strength on the Reorganizational Energy and Intramolecular

- Electron Transfer in Cytochrome B5 Labeled with Ruthenium(II) Polypyridine Complexes. *J Am Chem Soc* **1994**, *116* (16), 7356–7362. https://doi.org/10.1021/JA00095A045/SU PPL FILE/JA7356.PDF.
- (65) Schmit, J. D.; Kariyawasam, N. L.; Needham, V.; Smith, P. E. SLTCAP: A Simple Method for Calculating the Number of Ions Needed for MD Simulation. *J Chem Theory Comput* **2018**, *14* (4), 1823–1827. https://doi.org/10.1021/ACS.JCTC.7B012 54.
- (66) Loche, P.; Steinbrunner, P.; Friedowitz, S.; Netz, R. R.; Bonthuis, D. J. Transferable Ion Force Fields in Water from a Simultaneous Optimization of Ion Solvation and Ion-Ion Interaction. *Journal of Physical Chemistry B* 2021, 125 (30), 8581–8587.

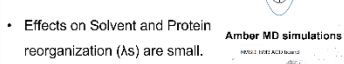
- https://doi.org/10.1021/ACS.JPCB.1C053 03/ASSET/IM-AGES/LARGE/JP1C05303_0004.JPEG.
- (67) Joung, I. S.; Cheatham, T. E. Determination of Alkali and Halide Monovalent Ion Parameters for Use in Explicitly Solvated Biomolecular Simulations. *Journal of Physical Chemistry B* 2008, *112* (30), 9020–9041. https://doi.org/10.1021/JP8001614/SUPPL FILE/JP8001614-FILE003.PDF.
- (68) Roe, D. R.; Cheatham, T. E. PTRAJ and CPPTRAJ: Software for Processing and Analysis of Molecular Dynamics Trajectory Data. *J Chem Theory Comput* **2013**, *9* (7), 3084–3095. https://doi.org/10.1021/ct400341p.

TOC Graphic

CYPWare 1.0: Mechanisms of ET modulations in CYP450 BM3

Ligand binding lowers ET ΔG°

 Mutations marginally increases ET ΔG°



 Buffer ions stabilize the reduced Heme state.

